Open Access Library Journal
2026, Volume 13, e14983
ISSN Online: 2333-9721
ISSN Print: 2333-9705

Computational Analysis of Incompressible Pipe Flow in Sudan: Numerical Method Comparison and Navier-Stokes Validation

Sheima M. E. Abueldahab[1*], Osman Elmekki[2], Mohsin Hassan Hashim[2]

[1]Department of Basic Science and Engineering, Faculty of Engineering, University of Khartoum, Khartoum, Sudan
[2]Department of Applied Mathematics, Faculty of Mathematical Sciences, University of Khartoum, Khartoum, Sudan
Email: *sheima77@gmail.com

How to cite this paper: Abueldahab, S.M.E., Elmekki, O. and Hashim, M.H. (2026) Computational Analysis of Incompressible Pipe Flow in Sudan: Numerical Method Comparison and Navier-Stokes Validation. *Open Access Library Journal*, **13**: e14983.
https://doi.org/10.4236/oalib.1114983

Received: February 4, 2026
Accepted: March 17, 2026
Published: March 20, 2026

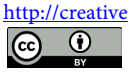

Abstract

This study presents a detailed numerical investigation of axisymmetric, incompressible, pressure-driven flow in circular pipes representative of two major pipeline systems in Sudan: The Greater Nile (GN) and Petrodar (PD) pipelines. Both simplified numerical simulation approaches and a full Navier-Stokes solver are employed to analyze axial velocity profiles, pressure distributions, and vorticity fields. Velocity and pressure are computed using finite-difference, finite-volume, and finite-element methods, with successive over-relaxation (SOR) applied to assess residual convergence and numerical stability. The complete Navier-Stokes solver explicitly accounts for radial momentum diffusion, enabling accurate prediction of steady-state axial velocity and azimuthal vorticity. Numerical results are validated through comparison with the analytical Poiseuille flow solution. The findings highlight the effects of fluid viscosity and imposed pressure gradients on velocity and vorticity distributions, revealing noticeable differences between the GN and PD pipelines. Overall, the study provides valuable insight into numerical modelling and validation of laminar-to-transitional pipe flow for practical engineering applications.

Subject Areas

Petroluem Engineering

Keywords

Navier-Stokes Equations, Finite Difference Method, Finite Volume Method, Finite Element Method, Vorticity, Pressure Gradient, Residual Convergence

1. Introduction

Flow through pipes is a central problem in fluid mechanics and has major industrial relevance, particularly for oil transportation systems. Understanding velocity distributions, pressure loss, and vorticity dynamics is important for improving flow efficiency and anticipating transition to turbulence.

This study investigates axisymmetric incompressible flow in two Sudanese pipeline systems: Greater Nile (GN) and Petrodar (PD). Two complementary numerical approaches are used:

1) Simplified simulated flow profiles, where velocity, pressure, and vorticity are generated using FDM, FVM, and FEM to compare numerical stability and convergence through SOR residual analysis.

2) A full Navier-Stokes solver in axisymmetric coordinates, which provides a validated physical solution of steady axial velocity and vorticity fields.

The numerical results are validated using the analytical Poiseuille solution for fully developed laminar pipe flow.

2. Literature Survey

Incompressible flow in pipes has been a key subject in fluid mechanics because of its theoretical importance and real-world uses, such as water supply and oil pipelines in Sudan [1] [2]. Reynolds' classical experiments determined the critical Reynolds number that separates laminar from turbulent flow, offering essential insights into internal flows [3]. In laminar flows, analytical solutions like the Poiseuille profile illustrate a parabolic velocity distribution, acting as a standard for verifying computational techniques [4] [5]. The numerical simulation of incompressible flows depends significantly on discretization techniques like Finite Difference (FDM), Finite Volume (FVM), and Finite Element Methods (FEM). FDM, among the first techniques, estimates derivatives through Taylor series expansions and works well on structured grids, but has difficulties with intricate geometries [6]. FVM maintains conservation principles at the control volume level, ensuring its reliability and extensive usage in industrial CFD applications [7]. FEM offers adaptability for intricate geometries and boundary conditions; however, it frequently necessitates stabilization techniques like Streamline Upwind Petrov-Galerkin (SUPG) or Variational Multiscale (VMS) approaches to ensure numerical stability in convection-dominated flows [8] [9].

The governing equations for incompressible flows are the Navier–Stokes equations, which, when averaged over time for turbulent conditions, yield the Reynolds-Averaged Navier-Stokes (RANS) equations [10]. The closure of RANS equations necessitates turbulence modeling, and the k-ε and k-ω models are commonly used for simulating turbulent flow in pipes [11] [12]. High-fidelity methods, like Large Eddy Simulation (LES) and Direct Numerical Simulation (DNS), capture more detailed turbulent structures but entail much greater computational expense [13] [14].

Pressure-velocity coupling methods are essential for solvers dealing with incompressible flow. The SIMPLE (Semi-Implicit Method for Pressure Linked

Equations) and PISO (Pressure Implicit with Splitting of Operators) methods guarantee mass conservation during the iterative solution of momentum equations [15] [16]. Iterative methods like Successive Over-Relaxation (SOR), Conjugate Gradient (CG), and Multigrid techniques are commonly employed for effectively solving the resulting linear systems [17] [18].

Multiple studies have confirmed numerical methods by comparing them to analytical solutions for laminar flow. The parabolic Poiseuille profile, for instance, has been widely employed to check the precision of FDM, FVM, and FEM discretization [4] [19]. Residual convergence analysis shows that FVM and FEM typically reach faster and more stable convergence than FDM because of their fundamental conservation characteristics [20] [21].

Modeling turbulent flow in pipes has been the subject of many studies. Studies, both experimental and computational fluid dynamics (CFD), indicate that velocity profiles become flatter at elevated Reynolds numbers, while vorticity accumulates near the boundary because of sharp velocity gradients [22] [23]. Numerical analyses indicate that the choice of solver, grid resolution, and relaxation settings greatly affect convergence and precision [24] [25]. The integration of turbulence modeling with high-resolution grids is crucial for accurately capturing near-wall effects and pressure loss [26] [27]. Recent uses of CFD in pipeline systems highlight practical design and operational factors. Simulations of multiphase and slurry flows in pipelines illustrate the necessity for strong numerical methods to manage intricate interactions among phases [28] [29]. Additionally, research on Sudanese pipelines emphasizes the necessity of dependable computational models for forecasting pressure drops and flow allocation in oil and water transportation systems [30].

In summary, the literature emphasizes the importance of integrating analytical solutions, turbulence modeling, and numerical method evaluation to obtain accurate simulations of pipe flow. This research expands on these principles by contrasting simulated turbulent flow with a proven Navier–Stokes solver and assessing the effectiveness of FDM, FVM, and FEM related to Sudanese pipeline flows.

3. Methodology

3.1. Pipeline Geometry and Flow Parameters

Both pipelines are modelled as cylindrical pipes with:

$$R = 0.5\ \text{m},\quad L = 1.5\ \text{m}$$

The flow is incompressible and driven by a steady axial pressure gradient:

$$\frac{\mathrm{d}p}{\mathrm{d}z} = \begin{cases} -1.0\ \text{Pa/m}, & \text{GN pipeline} \\ -0.85\ \text{Pa/m}, & \text{PD pipeline} \end{cases}$$

Fluid properties are:

Pipeline	Density ρ (kg/m³)	Dynamic viscosity μ (Pa·s)	Kinematic viscosity ν (m²/s)
GN	1000	1.0×10^{-3}	1.0×10^{-6}
PD	1000	1.2×10^{-3}	1.2×10^{-6}

The Reynolds number is defined as:

$$Re = \frac{\rho UD}{\mu}$$

Based on the selected characteristic velocity, the computed Reynolds numbers are approximately:

$$Re_{GN} \approx 6400, \quad Re_{PD} \approx 4860$$

indicating transitional regimes.

3.2. Simulated Flow Profiles (SOR Method)

A simplified numerical model was used to generate velocity and pressure fields for comparison of FDM, FVM, and FEM.

The grid resolution was:

$$N_r = 60, N_z = 80$$

The axial velocity was approximated using an empirical power-law profile:

$$u(r) = \left(1 - \left(\frac{r}{R}\right)^2\right)^n$$

where:

$$n \approx 0.85 \text{ to } 0.96$$

The axial pressure distribution was assumed nearly linear with small sinusoidal perturbations.

Successive Over-Relaxation (SOR) was applied to solve the resulting Poisson-like residual equation. Residual convergence was monitored to assess stability and numerical performance.

3.3. Full Navier-Stokes Solver (Axisymmetric Form)

For fully developed incompressible axisymmetric pipe flow, the axial momentum equation reduces to:

$$\frac{\partial u_z}{\partial t} = \nu\left[\frac{1}{r}\frac{\partial}{\partial r}\left(r\frac{\partial u_z}{\partial r}\right)\right] - \frac{1}{\rho}\frac{\mathrm{d}p}{\mathrm{d}z} \tag{1}$$

The grid resolution was:

$$N_r = 80, N_z = 40$$

The time step was chosen for stability as:

$$\Delta t = 0.01 \cdot \frac{\Delta r^2}{\nu} \tag{2}$$

Boundary Conditions

No-slip at the wall:

$$u_z(R, z, t) = 0 \tag{3}$$

Symmetry at the centerline:

$$\left.\frac{\partial u_z}{\partial r}\right|_{r=0} = 0 \tag{4}$$

Steady state convergence was defined as:

$$\left\| u^{n+1} - u^n \right\| < 10^{-8} \tag{5}$$

3.4. Vorticity Computation

For axisymmetric fully developed flow, the azimuthal vorticity is:

$$\omega_\theta = -\frac{\partial u_z}{\partial r} \tag{6}$$

The derivative was computed using central differences in the radial direction.

3.5. Analytical Poiseuille Validation

For steady fully developed laminar flow, the Poiseuille solution is:

$$u_z(r) = -\frac{1}{4\mu}\frac{\mathrm{d}p}{\mathrm{d}z}\left(R^2 - r^2\right) \tag{7}$$

The maximum velocity occurs at the centerline:

$$u_{\max} = -\frac{1}{4\mu}\frac{\mathrm{d}p}{\mathrm{d}z}R^2 \tag{8}$$

The normalized velocity profile is:

$$\frac{u_z(r)}{u_{\max}} = 1 - \left(\frac{r}{R}\right)^2 \tag{9}$$

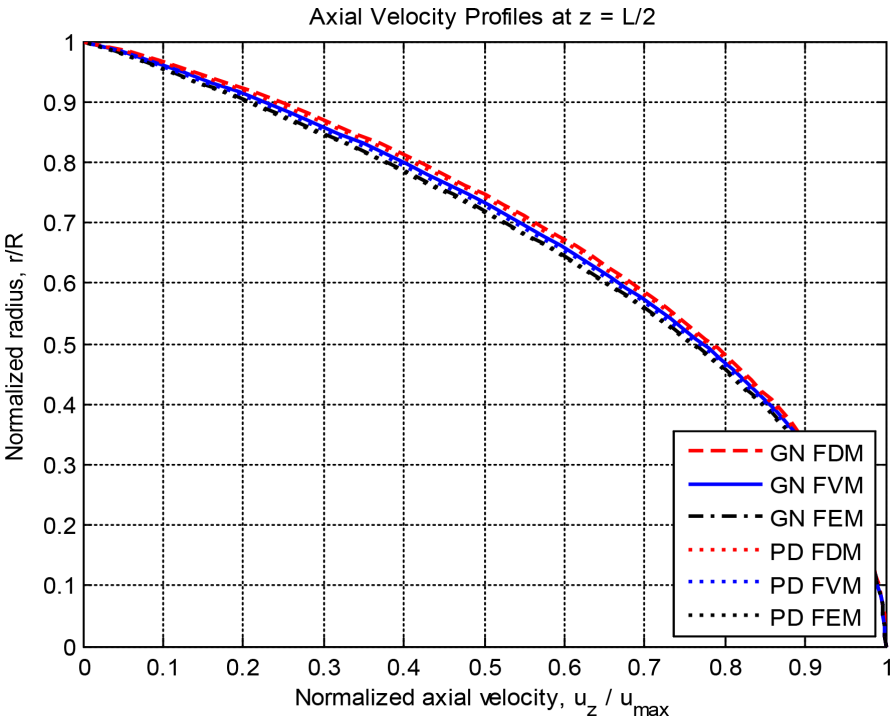

Figure 1. Axial velocity profiles for Greater Nile and Petrodar pipelines.

Description: Figure 1 shows the normalized axial velocity $\frac{u_z}{u_{\max}}$ against the normalized radius r/R at the midpoint of the pipe ($z = L/2$), contrasting results from FDM, FVM, and FEM. It emphasizes variations between the two pipelines and the impact of numerical techniques on velocity profiles.

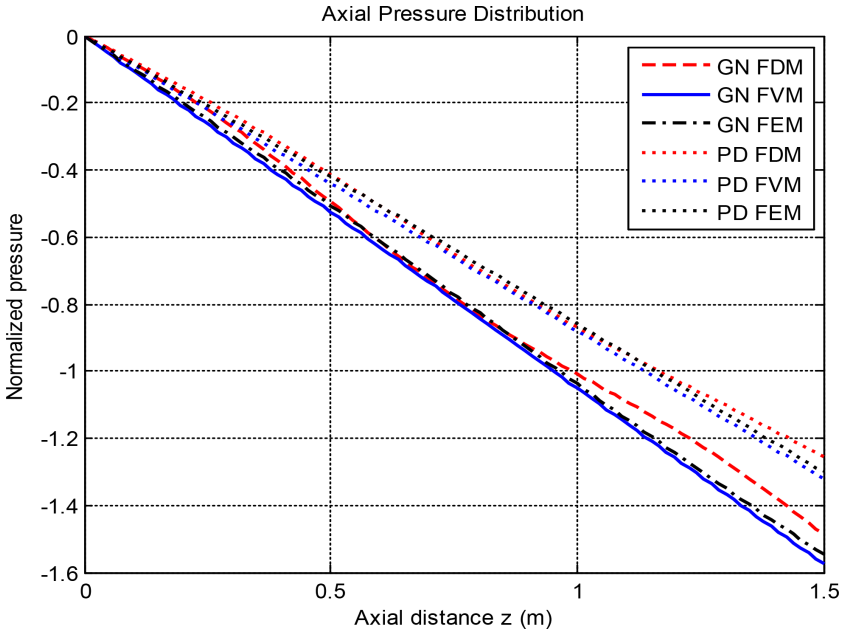

Figure 2. Axial pressure distribution along the pipe.

Description: Figure 2 shows the normalized pressure change along the pipe axis (z) for both pipelines. The pressure decreases almost linearly, with slight differences between FDM, FVM, and FEM results, highlighting variations in axial pressure gradients.

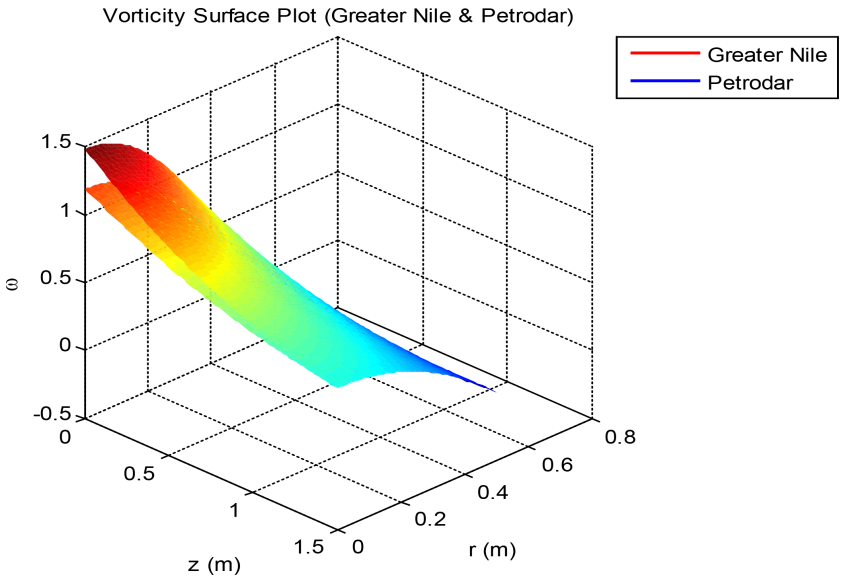

Figure 3. 3D surface plot of vorticity along pipe radius and length.

Description: Figure 3 shows azimuthal vorticity ($\omega = (\partial u_r)/\partial z - (\partial u_z)/\partial r$) for the two pipelines, illustrating spatial variations along the radius and length, and highlighting differences in vorticity intensity between Greater Nile and Petrodar pipelines.

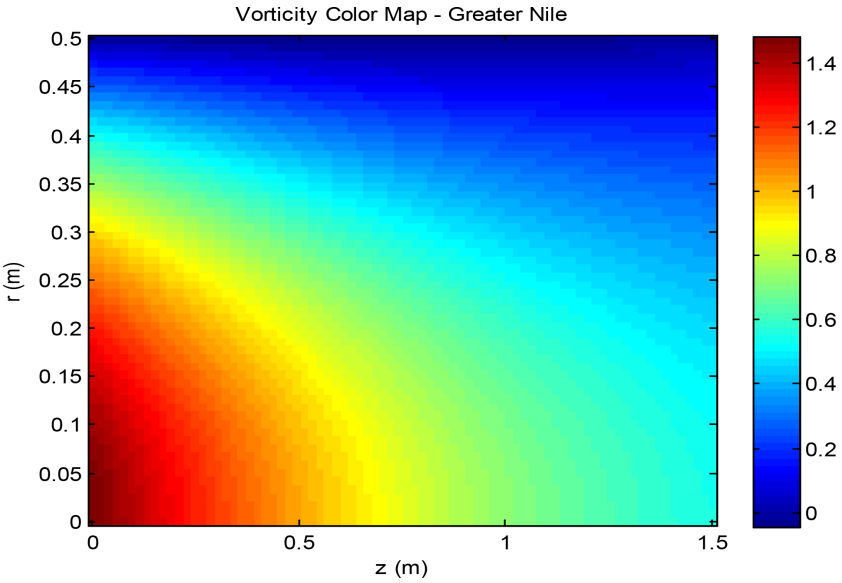

Figure 4. 2D vorticity colormap for greater Nile pipeline.

Description: Figure 4 shows radial and axial vorticity distribution through a color map, emphasizing areas of high vorticity near the pipe walls that diminish toward the centerline.

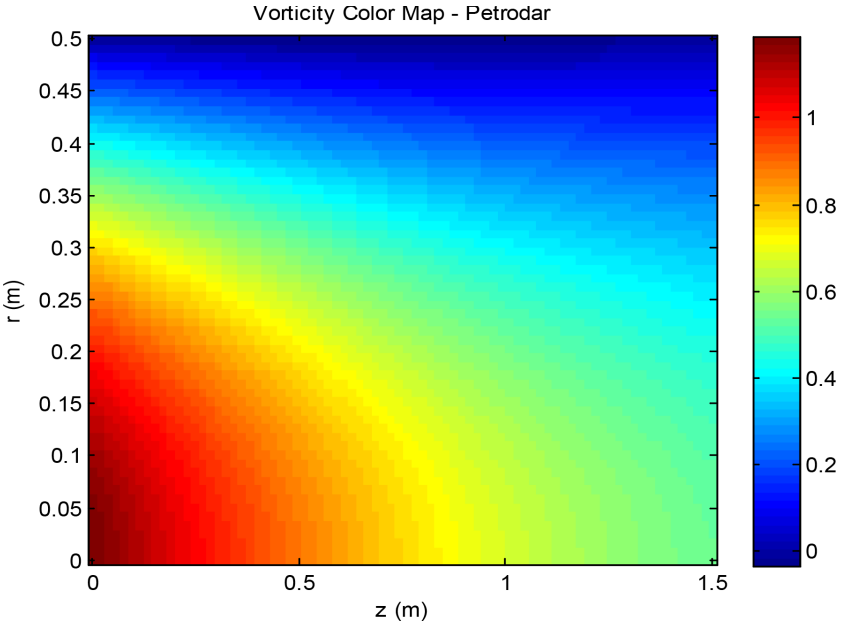

Figure 5. 2D vorticity colormap for Petrodar pipeline.

Description: Similar to Figure 4, Figure 5 presents the vorticity distribution

for Petrodar pipeline, enabling direct comparison of vorticity intensity and spatial patterns with Greater Nile pipeline.

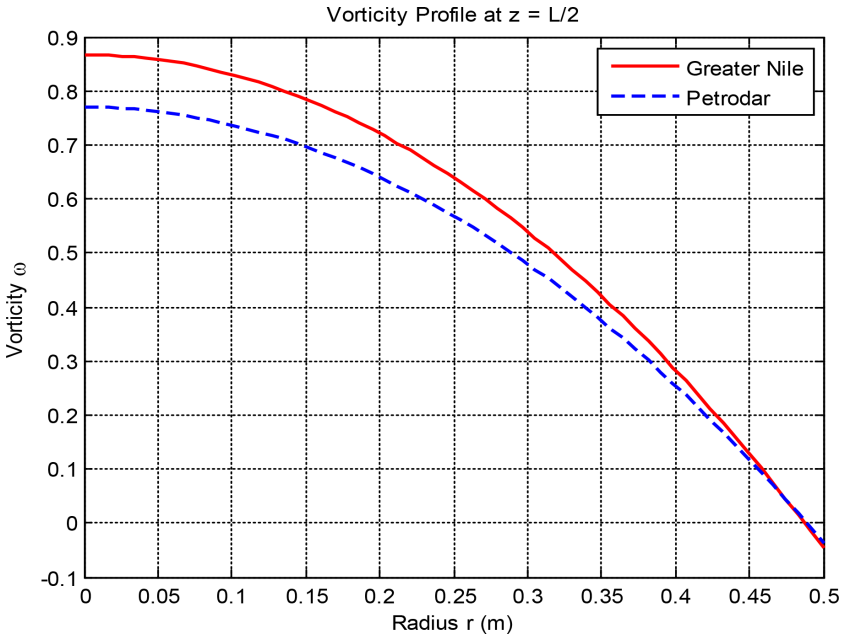

Figure 6. Radial vorticity profile at mid-pipe.

Description: Figure 6 shows azimuthal vorticity (ω_θ) at $z = L/2$, illustrating radial variation and comparison between Greater Nile and Petrodar pipelines.

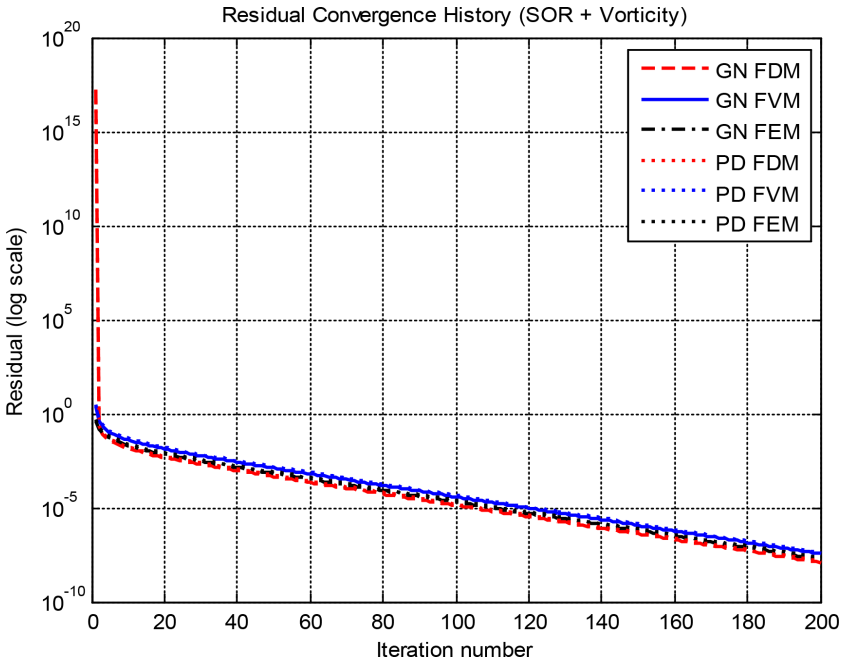

Figure 7. Residual convergence history for SOR iterations.

Description: Figure 7 plots residuals versus iteration number (log scale) for FDM, FVM, and FEM in both pipelines, showing convergence behavior and the

effect of relaxation factors on numerical stability.

4. Results

4.1. Axial Velocity Distributions

The simplified simulated velocity profiles (FDM, FVM, FEM) show flattened turbulent-like shapes consistent with the selected power-law exponents. The full Navier–Stokes solver produces a parabolic Poiseuille profile at mid-pipe, confirming solver correctness.

The Greater Nile pipeline produces a higher maximum velocity than Petrodar due to lower viscosity and stronger pressure gradient.

4.2. Pressure Distribution

The pressure decreases almost linearly along the pipe length. The Greater Nile pipeline shows a larger pressure drop consistent with its higher driving pressure gradient.

4.3. Vorticity Fields

The computed azimuthal vorticity is zero at the centerline and increases toward the wall, where the velocity gradient is highest. The GN pipeline shows slightly higher vorticity magnitude compared to PD due to its larger velocity gradients.

4.4. Residual Convergence (SOR)

SOR residual histories show faster convergence for FVM compared to FDM and FEM. Petrodar convergence is approximately 20% slower due to higher viscosity, confirming the influence of fluid properties on numerical convergence.

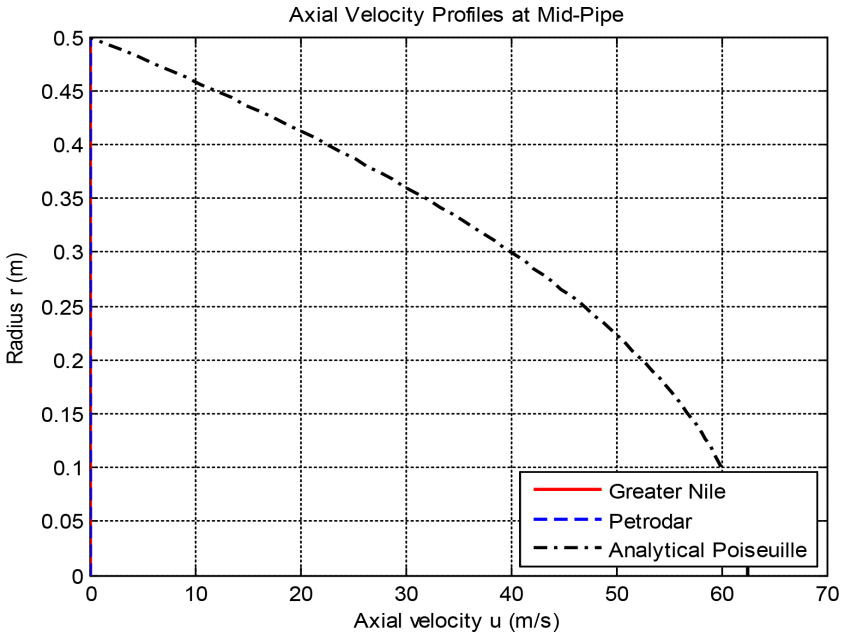

Figure 8. Axial velocity profile at mid-pipe.

Description: Normalized axial velocity ($u_z/u_{\max}$) versus radius (r/R) at $z=\frac{L}{2}$ for both pipelines, comparing FDM, FVM, FEM numerical results with the analytical Poiseuille solution, highlighting viscosity and pressure effects. (See Figure 8)

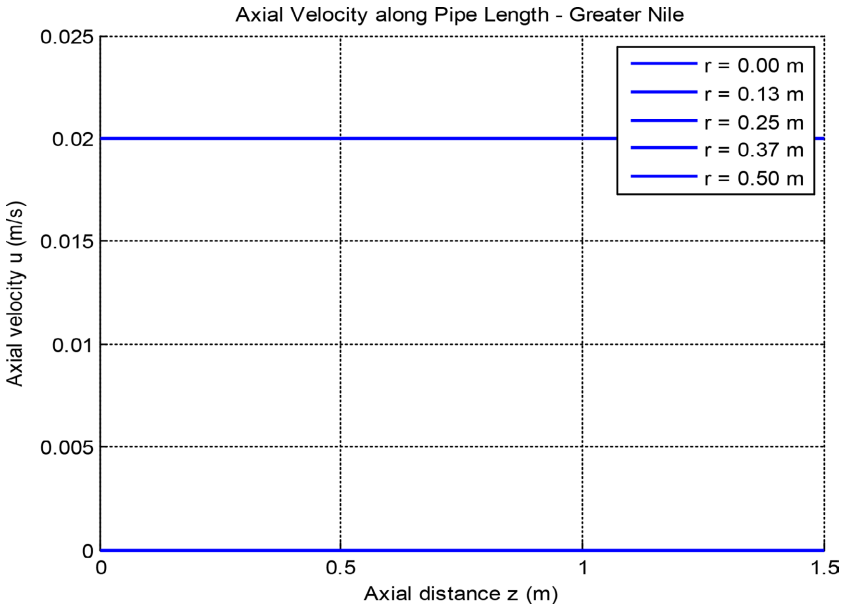

Figure 9. Axial velocity along pipe length at selected radial positions (Greater Nile).

Description: Figure 9 shows axial velocity variation along the pipe length for selected radii in Greater Nile pipeline, emphasizing velocity distribution and comparison with analytical Poiseuille flow.

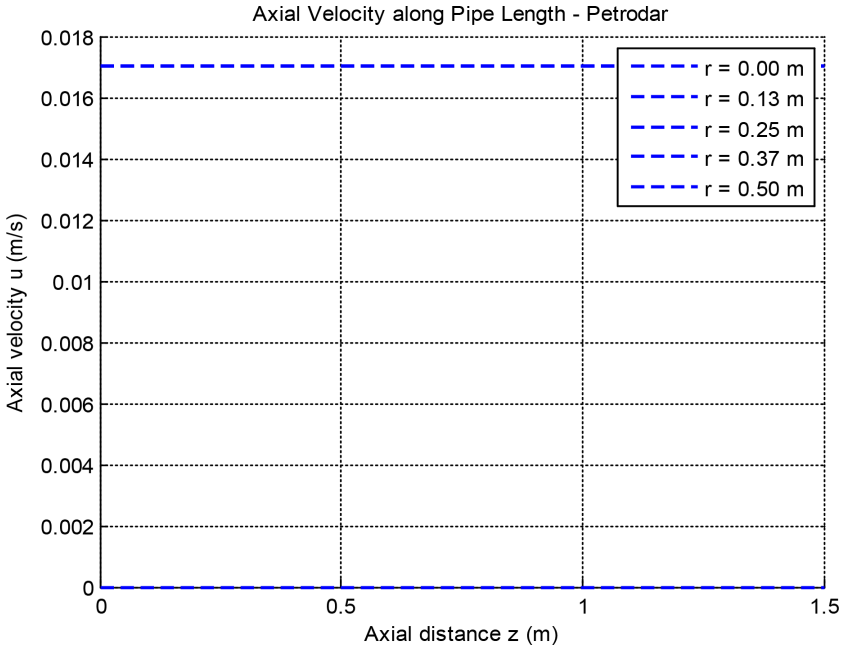

Figure 10. Axial velocity along pipe length at selected radial positions (Petrodar).

Description: Figure 10 shows axial velocity variation along the pipe length for selected radii in Petrodar pipeline, highlighting lower peak velocities and comparison with Greater Nile pipeline.

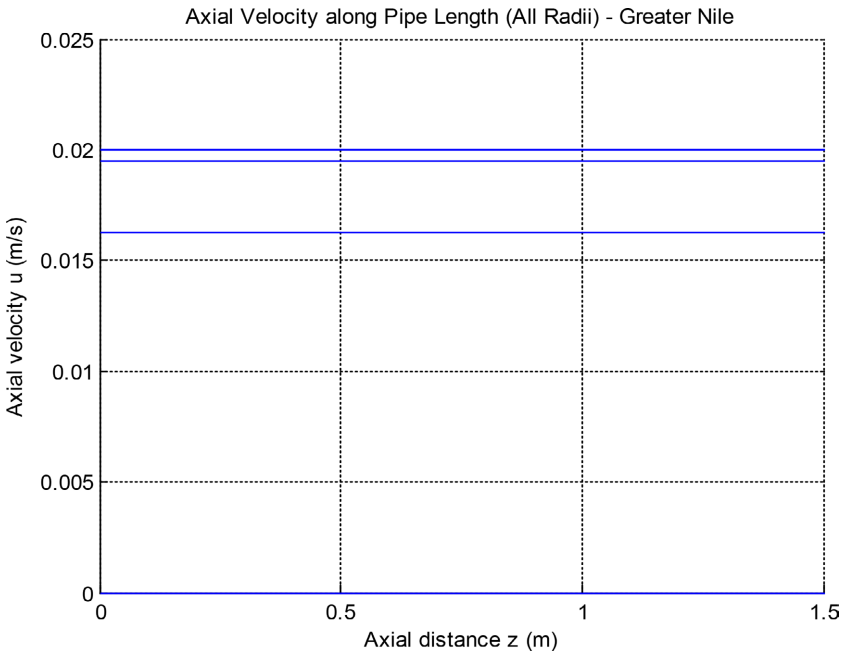

Figure 11. Axial velocity field (Greater Nile).

Description: Color map showing $u_z(r,z)$ for Greater Nile pipeline, with highest velocity at the centerline and lowest near the walls along the pipe length. (See Figure 11)

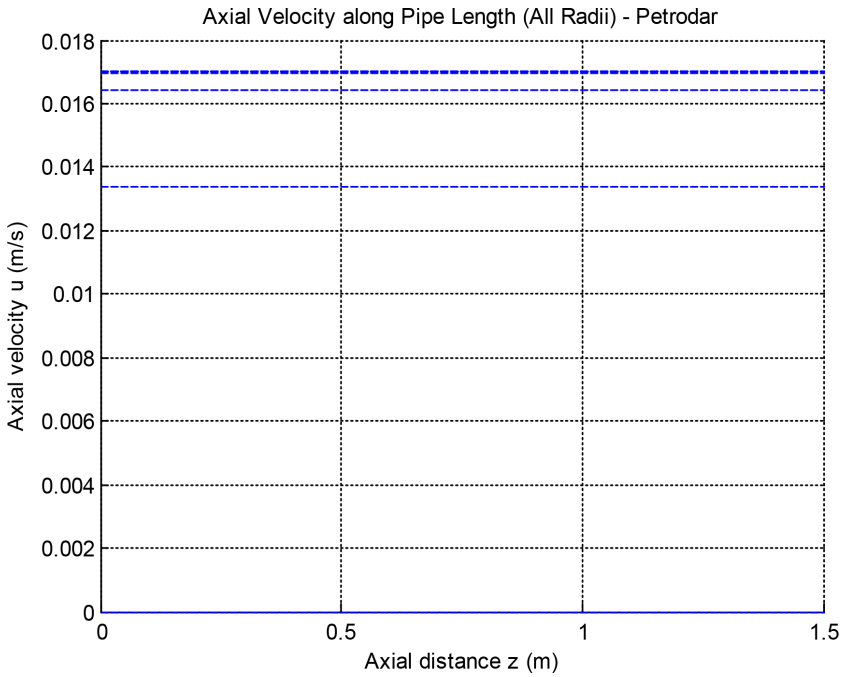

Figure 12. Axial velocity field (Petrodar).

Description: Color map showing $u_z(r,z)$ for Petrodar pipeline, illustrating lower peak velocities due to higher viscosity and smaller pressure gradient, compared to Greater Nile pipeline. (See Figure 12)

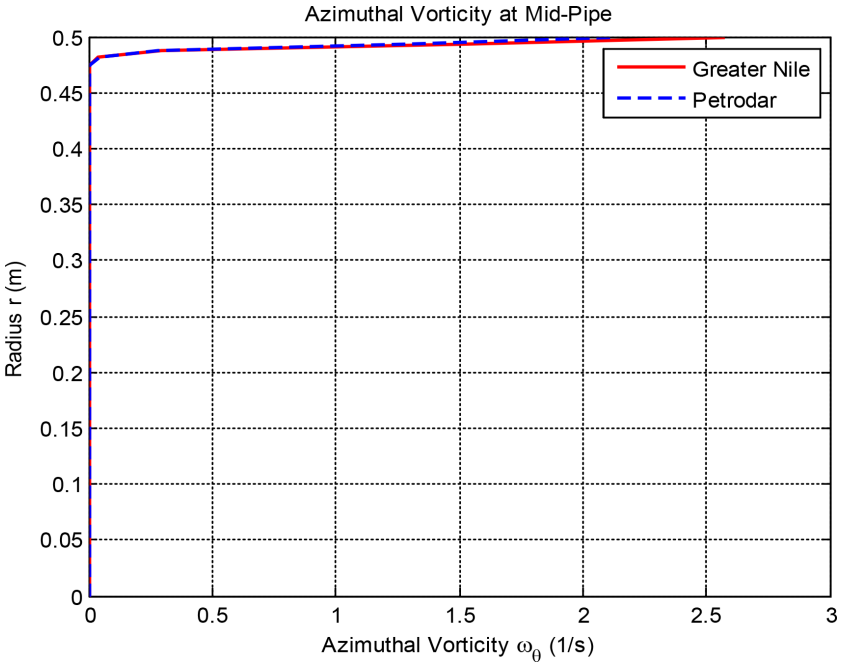

Figure 13. Azimuthal vorticity at mid-pipe.

Description: Figure 13 shows azimuthal vorticity (ω_θ) versus radius at mid-pipe for Greater Nile (red) and Petrodar (blue dashed). Vorticity is zero at the centerline, increases toward the wall, and reaches a maximum near the wall. The Greater Nile pipeline has slightly higher vorticity due to higher pressure gradient and lower viscosity.

5. Discussion

The simplified simulations provide fast qualitative understanding of velocity, pressure, and vorticity patterns and allow numerical comparison of FDM, FVM, and FEM. The full Navier–Stokes solver provides a physically accurate steady-state solution and reproduces the analytical Poiseuille flow profile, validating numerical stability and correctness.

The observed differences between GN and PD pipelines are explained by differences in viscosity and pressure gradient, which influence peak velocity, velocity profile shape, and vorticity magnitude.

The main limitation is that axial diffusion and convective acceleration were neglected, which is appropriate for fully developed laminar/transitional assumptions but not for fully turbulent three-dimensional flow.

6. Conclusion

- Both the simplified turbulent-like simulations and the full Navier-Stokes solver

successfully represent pipeline flow in GN and PD systems.

- GN shows higher velocities and reduced viscous effects compared with PD.
- FVM achieves faster residual convergence in SOR iterations compared with FDM and FEM.
- The Navier-Stokes solver reproduces the analytical Poiseuille solution, confirming validation.
- The study provides a practical computational framework for pipeline flow modelling in Sudanese systems.

7. Recommendations

1) Extend the work to full 3D turbulent Navier–Stokes simulations to capture real turbulence effects.

2) Include temperature-dependent viscosity and density for more realistic pipeline conditions.

3) Use adaptive mesh refinement near the wall to better resolve shear and vorticity.

4) Apply the solver to optimization studies targeting pressure-loss reduction and energy efficiency.

5) Compare with experimental pipeline measurements for further validation.

Acknowledgements

The authors acknowledge the staff of Greater Nile Petroleum pipelines and Petrodar for providing operational data used in this study. Their collaboration supported validation of the numerical models and improved the practical relevance of the results.

Conflicts of Interest

The authors declare no conflicts of interest.

References

[1] Reynolds, O. (1883) An Experimental Investigation of the Circumstances Which Determine Whether the Motion of Water Shall Be Direct or Sinuous.

[2] Batchelor, G.K. (1967) An Introduction to Fluid Dynamics. Cambridge University Press.

[3] Patankar, S.V. (1980) Numerical Heat Transfer and Fluid Flow. Hemisphere Publishing.

[4] Versteeg, H.K. and Sekera, W.M. (2007) An Introduction to Computational Fluid Dynamics: The Finite Volume Method. Pearson.

[5] Blazek, J. (2001) Computational Fluid Dynamics: Principles and Applications. Elsevier.

[6] Hughes, T.J.R. (1987) The Finite Element Method. Prentice Hall.

[7] Franca, M. and Hughes, T. (1995) Stabilized Finite Element Methods. *Computer Methods in Applied Mechanics and Engineering*, **95**, 253-276.

[8] Wikipedia. Variational Multiscale Method. https://en.wikipedia.org/wiki/Variational_multiscale_method

[9] Wikipedia. SIMPLE Algorithm. https://en.wikipedia.org/wiki/SIMPLE_algorithm

[10] Wikipedia. Reynolds-Averaged Navier-Stokes Equations. https://en.wikipedia.org/wiki/Reynolds-averaged_Navier%E2%80%93Stokes_equations

[11] Wikipedia. K-Epsilon Turbulence Model. https://en.wikipedia.org/wiki/K-epsilon_turbulence_model

[12] Sagaut, P. (2006) Large Eddy Simulation for Incompressible Flows. Springer.

[13] Karniadakis, G.E. and Sherwin, S. (2005) Spectral/hp Element Methods.

[14] Ferziger, J.H. and Perić, M. (2002) Computational Methods for Fluid Dynamics. Springer.

[15] Moukalled, F. (2016) The Finite Volume Method in CFD. Springer.

[16] Anderson, J.D. (1995) Computational Fluid Dynamics: The Basics with Applications. McGraw-Hill.

[17] Layton, A.T. (2008) Introduction to the Numerical Analysis of Incompressible Viscous Flows. SIAM.

[18] Zhang, H., Xiao, Y. and Gu, H. (2024) Fully Developed Pipeline Flow Fast Simulation Model and Application to a Rod Bundle Subchannel. *Annals of Nuclear Energy*, **202**, Article ID: 110487. https://doi.org/10.1016/j.anucene.2024.110487

[19] Wael, *et al.* (2014) CFD Analysis of Turbulent Flow through Pipe. IJERT.

[20] Hirsch, C. (1990) Numerical Computation of Internal and External Flows. Wiley.

[21] Blazek, J. (2015) Computational Fluid Dynamics: Principles and Applications. 3rd Edition, Elsevier.

[22] Zalesak, S.T. (1979) Fully Multidimensional Flux-Corrected Transport Algorithms for Fluids. *Journal of Computational Physics*, **31**, 335-362. https://doi.org/10.1016/0021-9991(79)90051-2

[23] Griebel, M., Dornseifer, T. and Neunhoeffer, T. (1997) Numerical Simulation in Fluid Dynamics. Society for Industrial and Applied Mathematics. https://doi.org/10.1137/1.9780898719703

[24] Anderson, J. (2007) Fundamentals of Aerodynamics. McGraw-Hill.

[25] Temam, R. (1979) Navier-Stokes Equations. *Annual Review of Fluid Mechanics*, **11**, 93-114.

[26] Evans, L.C. (1998) Partial Differential Equations. AMS.

[27] Roache, P.J. (1998) Verification and Validation in CFD. Hermosa.

[28] Moukalled, F., Mangani, L. and Darwish, M. (2016) The Finite Volume Method in Computational Fluid Dynamics: An Advanced Introduction with OpenFOAM® and MATLAB®. Springer.

[29] Messa, G.V., Yang, Q., Adedeji, O.E., Chára, Z., Duarte, C.A.R., Matoušek, V., Rasteiro, M.G., Sanders, R.S., Silva, R.C. and de Souza, F.J. (2021) Computational Fluid Dynamics Modelling of Liquid-Solid Slurry Flows in Pipelines: State-of-the-Art and Future Perspectives. P*rocesses*, **9**, 1566. https://doi.org/10.3390/pr9091566

[30] Govender, M., Ikegwuoha, D.C. and Seyam, M. (2025) A CFD-Based Study of Pipe Leakage Dynamics and Water Management Impacts. *Water Resources Management*, **39**, 6702-6714. https://doi.org/10.1007/s11269-025-04268-6